agronomy

MDPI

Article

A Precision Agriculture Approach for Durum Wheat Yield Assessment Using Remote Sensing Data and Yield Mapping

Piero Toscano [1], Annamaria Castrignanò [2], Salvatore Filippo Di Gennaro [1,*], Alessandro Vittorio Vonella [2], Domenico Ventrella [2] and Alessandro Matese [1]

1 Institute of BioEconomy (IBE), National Research Council (CNR), Via Caproni 8, 50145 Florence, Italy
2 Council for Agricultural Research and Economics, Research Centre for Agriculture and Environment (CREA-AA), Via Celso Ulpiani 5, 70125 Bari, Italy
* Correspondence: salvatorefilippo.digennaro@cnr.it; Tel.: +39-055-3033711

Received: 19 July 2019; Accepted: 3 August 2019; Published: 8 August 2019

Abstract: The availability of big data in agriculture, enhanced by free remote sensing data and on-board sensor-based data, provides an opportunity to understand within-field and year-to-year variability and promote precision farming practices for site-specific management. This paper explores the performance in durum wheat yield estimation using different technologies and data processing methods. A state-of-the-art data cleaning technique has been applied to data from a yield monitoring system, giving a good agreement between yield monitoring data and hand sampled data. The potential use of Sentinel-2 and Landsat-8 images in precision agriculture for within-field production variability is then assessed, and the optimal time for remote sensing to relate to durum wheat yield is also explored. Comparison of the Normalized Difference Vegetation Index(NDVI) with yield monitoring data reveals significant and highly positive linear relationships (r ranging from 0.54 to 0.74) explaining most within-field variability for all the images acquired between March and April. Remote sensing data analyzed with these methods could be used to assess durum wheat yield and above all to depict spatial variability in order to adopt site-specific management and improve productivity, save time and provide a potential alternative to traditional farming practices.

Keywords: yield mapping; remote sensing; durum wheat; precision agriculture

1. Introduction

Durum wheat (*Triticum durum*, Desf.), although it represents only 8% of global wheat production, is one of the most common cereal crops in the Mediterranean basin, traditionally grown under rainfed conditions using conventional tillage [1–3]. Climate variability, price volatility and socio-economic factors are the main sources of uncertainty and concern for farmers in durum wheat cultivation [4,5]. For climate variability, it was shown how, in rainfed conditions, these affected both the quality and quantity of durum wheat production [6]. For other crops, evidence was given by Bowman and Zilberman [7] of how both price volatility and socio-economic factors might influence the agronomic techniques adopted. In light of this, it is increasingly urgent to provide information to optimize crop management and estimate crop yields before harvest for a sustainable agricultural income and ensuring food security. Precision agriculture (PA) has been used for ≥25 years to optimize the use of farm inputs such as fertilizers and herbicides [8,9], and thus maximize profit and minimize negative environmental impacts [10] by addressing spatial variability.

Yield mapping is one of the most widely-used precision agriculture techniques [11–13]. Most of these datasets are characterized by a non-normal distribution due to the presence of errors and outliers and can be misleading if used for decision making processes. Over the last 25 years, several studies have analyzed the sources of errors that cause this non-normality and proposed different processing techniques to reduce their effect [11,14,15]. However, among the studies highlighting accuracy issues associated with the use of the yield monitoring systems, only one compared yield monitoring with hand sampled data [16].

During the same period many studies have been published using satellite imagery to estimate crop parameters and yields [17–19], many of these using empirical relationships between yields and various vegetation indices (VIs) with limited applicability to different areas or years [9], especially in the recent era of prolific satellite data availability [20].

In the last years many studies have focused on the use of medium resolution satellite data (10–100 m) for yield estimation at broader spatial resolution (local, regional, country scales) even for long-term yield series analysis [20–26]. While studies are conducted by the use of very high resolution imagery [27–30] to identify within-field variability of crop growth and yield and for the definition of management zones, few [31] have used Sentinel-2 to provide an insight into field productivity variation for better future management [32–34]. The objectives of this study were to:

- Evaluate the correctness of yield monitoring maps comparing them with hand sampled yield data;
- Evaluate the ability of the most commonly used VI (NDVI) calculated from Landsat-8 and Sentinel-2 satellite platforms to understand within-field variability;
- Understand the optimal time for NDVI acquisition for better yield evaluation;
- Evaluate the relations between NDVI and yield for four durum wheat crop seasons with different climatic conditions and yield performance.

For the last two points, given the scarcity of satellite images, a durum wheat simulation model [5] was used to reconstruct the crop growth variables and analyze in detail the differences that emerged in the yield-NDVI correlation for the four crop seasons.

2. Materials and Methods

2.1. Study Site and Field Trial

The research was performed at the Menichella Experimental Farm of CREA-AA (Council for Agricultural Research and Economics—Research Centre for Agriculture and Environment), located in the Foggia countryside (Southern Italy, 41°27′05.9″ N, 15°30′43.6″ E; 88 m a.s.l.), within the study area of the JECAM site (http://jecam.org/studysite/italy-apulian-tavoliere/), during the 2013–2014, 2014–2015, 2015–2016 and 2016–2017 crop seasons. This study was conducted on a 5 ha field cropped with rainfed durum wheat (*Triticum durum*, Desf., cv Claudio) under conventional management and continuous cultivation.

The field is in a flat area called 'Apulian Tavoliere' and the soil is silty-clay Vertisol of alluvial origin classified as Fine Mesic Typic Cromoxerert by Soil Taxonomy USDA [35].

The soil in the upper 60 cm layer has a good availability of total nitrogen (0.12 g 100 g^{-1}), organic matter (2.07 g 100 g^{-1}) and 41 mg kg^{-1} of available phosphorus (P_2O_5). In summer 4–5 cm wide cracks frequently appear from the surface to about 50 cm depth.

The climate is classified as Mediterranean subtropical with a thermic soil temperature regime. Rainfall, unevenly distributed throughout the seasons and with a long-term annual average of 550 mm, is mostly concentrated in the winter months, while the dry period is from May to September [36]. Daily weather parameters (air temperature, relative humidity, global solar radiation, rainfall and wind speed), were recorded at the agro-meteorological station of the CNR-IBE weather station network (Foggia, 41°30′00.4″ N, 15°30′46.4″ E, 69 m a.s.l.). The field has been cultivated with a common agronomic management, applying 36 kg ha^{-1} of N as diammonium phosphate (18–46) before sowing and 68.4 kg ha^{-1} as ammonium nitrate (34.2) as top dressing at the end of tillering stage.

Sowing date varied between November and December due to the weather conditions (12 December 2013, 20 November 2014, 19 November 2015 and 29 November 2016). In each cropping season, the sowing density was of 350 germinable seeds/m^2 with 15 cm row spacing.

2.2. Hand Yield Samplings and Yield Map Monitoring

At maturity stage of each season aboveground biomass was collected over 1 m^2 areas in proximity to the 104 sampling points at the nodes of a 20 × 20 m cell-grid (Figure 1). The points were georeferenced in UTM coordinates WGS 84 using a TOPCON GPS, differentially corrected with an accuracy of less than one meter. All measurements were repeated at the same points over the years.

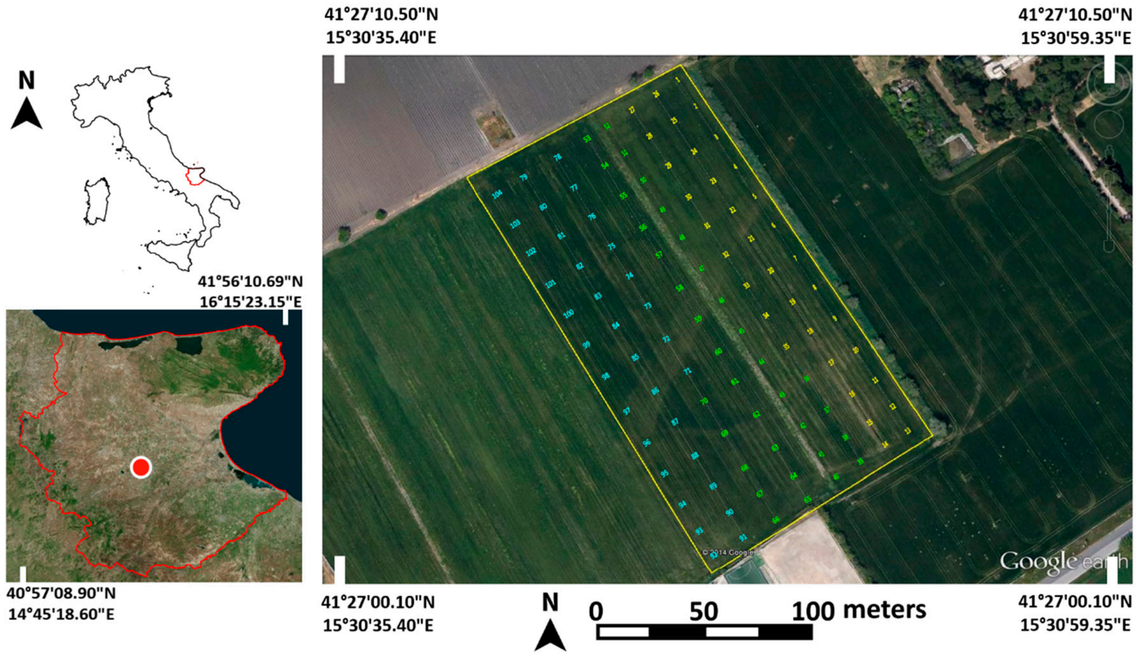

Figure 1. Location of study site and 104 sampling points.

At harvesting in 14 July 2014, 29 June 2015 and 12 July 2016, yield data were recorded by external services provider with a John Deere T670i combine (Deere & Company, Moline, USA) equipped with a yield monitor system (grain mass flow and moisture sensors). The data were recorded every second, which produced a support (footprint) of 6 × 1 m^2 depending on the forward speed of the machine.

For 2017, the last year of analysis, a yield monitoring map was unavailable. The data were measured only at the 104 sampling points.

2.3. Satellite Data

Remote sensing images acquired by the Operational Land Imager (OLI) instrument aboard the Landsat-8 satellite and by the Multi-Spectral Instrument (MSI) aboard the Sentinel-2A satellite were used in the study. Landsat-8/OLI captures images of the earth's surface in nine spectral bands at 30 m spatial resolution (15 m for panchromatic band) while Sentinel-2A/MSI captures images in 13 spectral bands at 10 m, 20 m and 60 m spatial resolution. After cloud and shadow screening, a total of 11 Landsat-8 and five Sentinel-2A (Table 1 images of the study area from 1 March 2013 to 1 June 2017 were selected.

Table 1. Acquired dates of Landsat-8 and Sentinel-2 (2014–2017).

	LANDSAT-8	SENTINEL-2
2014	19 March, 20 April	NA
2015	14 April, 30 April	NA
2016	13 March, 9 April, 18 May, 27 May	23 May
2017	2 March, 12 April, 30 May	9 March, 29 March, 8 April, 18 May

The Landsat-8/OLI images were downloaded using USGS (earthexplore.com) that provides data corrected from atmospheric effects.

Sentinel-2A/MSI images were atmospherically corrected for surface reflectance using the European Space Agency's (ESA) Sen2Cor algorithm (http://step.esa.int/main/third-party-plugins-2/sen2cor), which processes ESA's Level-1C top-of-atmosphere reflectance to atmospherically-corrected bottom-of-atmosphere (BoA) reflectance (Level-2A).

Lastly, NDVI [37] was calculated for Landsat-8 images using band 5 (NIR) and band 4 (RED), and for Sentinel-2A images using band 8 (NIR) and band 4 (RED) according to the formula:

$$NDVI = (NIR - RED)/(NIR + RED) \tag{1}$$

Providing two estimates with different support: 30×30 m^2 for Landsat-8 and 10×10 m^2 for Sentinel-2A.

2.4. Data Analysis

Yield map data were firstly normalized to 13% grain moisture content (hereinafter referred to as raw data) and then processed following the Vega et al. [13] protocol. The geographic coordinates of each dataset were converted into UTM Cartesian coordinates, specifying the zone (33, north) and the ellipsoid (WGS84). The 3 years maps in shapefile format (SHP) were pre-processed following a workflow using GeoDa software [38] for Moran index calculation for outliers identification, QGIS [39] for vegetation indices (VIs) calculation, Vesper software [40] for geostatistical interpolation, Matlab [41] for data statistical analysis.

Yield monitoring data underwent a pre-processing procedure in order to automatically identify and delete incorrect values through the two following steps suggested by Vega et al. [13].

Step 1: A threshold was applied by removing the yield values of less than 0.1 t/ha and then yield data points up to 10 m from the edge were removed in order to avoid edge effects. Lastly, yield data out of mean ±3 SD were automatically detected and deleted. This filter was used to prevent changes in inflation as a result of an incorrect estimate of very low data.

Step 2: Moran's local index of spatial autocorrelation and Moran's plot were applied to detect spatial outliers [42,43].

Lastly, the yield map for each year and dataset was assessed separately (raw data, Step1 and Step1 + Step2) by means of ordinary kriging, evaluating spatial variability using a semivariogram of the variable (yield monitoring).

Vesper software was used and an exponential model was fitted to the experimental variogram and model parameters: Nugget (micro-scale variation or measurement error), sill (asymptotic value approximately corresponding to sample variance) and effective range (distance at which 95% sill is reached) were estimated.

Yield values from the prediction map based on raw yield data and Step1 + Step2 yield data were then extracted in the neighborhood (3 m radius) of 104 yield sampled grid points and compared with them.

Step1 + Step2 yield monitoring data were interpolated using block kriging over a block of 10 × 10 m^2 or 30 × 30 m^2 to assess the spatial relationship between yield and the two types of remote sensing data (Sentinel-2A and Landsat-8, respectively) and to report on the optimal timing at which spectral measurements should be taken in durum wheat to maximize the correlation with yield (2014, 2015, 2016). The same procedure was adopted for hand yield samplings (block of 10 × 10 m^2 or 30 × 30 m^2) to assess the spatial relationship between yield and remote sensing data for 2017.

The Pearson coefficient, which is an index that measures the degree of correlation between linearly related variables and ranges between −1 and +1, was used to assess the linear relationship between yield monitoring data and yield sampling data, and between the NDVI and yield monitoring data.

For each regression analysis the correlation coefficient, regression coefficients (intercept and slope) and their corresponding probability levels were estimated, to test the statistical significance (null hypothesis equal to zero).

The performance of the protocol for automating error removal from yield monitoring data was evaluated using the root-mean-square error (RMSE).

2.5. Modelling

To better understand the correlations between remote sensing data and yield and go into detail about crop development and spectral signature, we used the Delphi crop growth model to perform field-scale simulations. The Delphi model was chosen due to the recent validations of its ability to simulate crop growth, yield and product quality conducted in the same study area [1,5]. The Delphi model is based on a FORTRAN-based mechanistic model [44] calibrated for durum wheat in Mediterranean conditions. Plant transpiration and soil evaporation, water and nitrogen soil-plant cycle are incorporated in the model. Input weather data at daily time scale are: Air temperature (maximum, minimum and average), global shortwave radiation, rainfall, wind speed (average) and relative humidity (average). Input data of the main physiological parameters of the durum wheat cultivar, sowing date and number of seeds/m^2, the soil hydrological profile, soil total nitrogen content profile, agronomic data on quality and quantity of nitrogen and roots growth data are also required.

Due to the strong correlation between leaf area index (LAI) and aboveground dry biomass [45], because aboveground dry biomass of plants generally determines LAI, the Delphi model was implemented to calculate LAI for each crop season. The model also predicted the heading, anthesis, maturity dates and length of time between these phases.

These pieces of information were used for detailed analysis of interannual variability and to better understand the different relationships between yield and NDVI over the years.

The weather data input to perform the Delphi simulation were acquired by the weather station located at Foggia, 41°30′00.4″ N, 15°30′46.4″ E, 69 m a.s.l., while sowing date, number of seeds/m^2 and nitrogen fertilization application data were set according to the data reported in Section 2.1. No changes were made to the Delphi model, as it had already been calibrated, validated and tested over 11 crop seasons for this region [5].

3. Results and Discussion

3.1. Yield Map and Yield Sample

A yield map is the basis for understanding yield variability within a field, analyzing its causes and improving management to increase profit [46].

A number of errors may be associated with common yield data collection: The yield monitor may not shut off at the field end and will register 0 value until harvestable crop again moves into the combine; the combine grain-flow system may plug temporarily, especially if the crop has lodged or weeds interfere with continuous grain flow; a time lag can occur between the time the crop is cut and the time its yield is measured in the grain flow [14,15,47]. Researchers have reported that 10% to 50% of observations reveal measurement errors [13,48].

The raw yield data of all three crop seasons used in this study showed high positive skewness coefficient (Table 2 and Figure 2). However, after Step1 and Step1 + Step2, the yield probability distributions were practically symmetric and the statistics were not biased by the presence of atypical data. After removing statistical outliers, the variable distribution tended to be more symmetric, without affecting the spatial structuring.

Table 2. Statistical features of yield monitoring datasets for uncleaned and cleaned yield data. Yield monitoring vs. yield sampling based on interpolated data.

Year	Number of Yield Monitoring Data			Skewness			Yield Monitoring vs. Yield Sampling	
	RAW	**Step1**	**Step2**	**RAW**	**Step1**	**Step2**	**RAW**	**Step1 + Step2**
2014	6369	4703 −26.2%	4641 −1.32%	17.72	2.72	2.71	$r = 0.11$ p-value = 0.25 RMSE = 1.14 t/ha	$r = 0.40$ p-value < 0.0001 RMSE = 1.05 t/ha
2015	6351	4737 −25.4%	4648 −1.88%	21.58	0.65	0.44	$r = 0.37$ p-value < 0.0001 RMSE = 0.68 t/ha	$r = 0.50$ p-value < 0.0001 RMSE = 0.59 t/ha
2016	6699	5084 −24.1%	4967 −2.30%	23.94	0.39	0.38	$r = 0.43$ p-value < 0.0001 RMSE = 0.84 t/ha	$r = 0.49$ p-value < 0.0001 RMSE = 0.82 t/ha

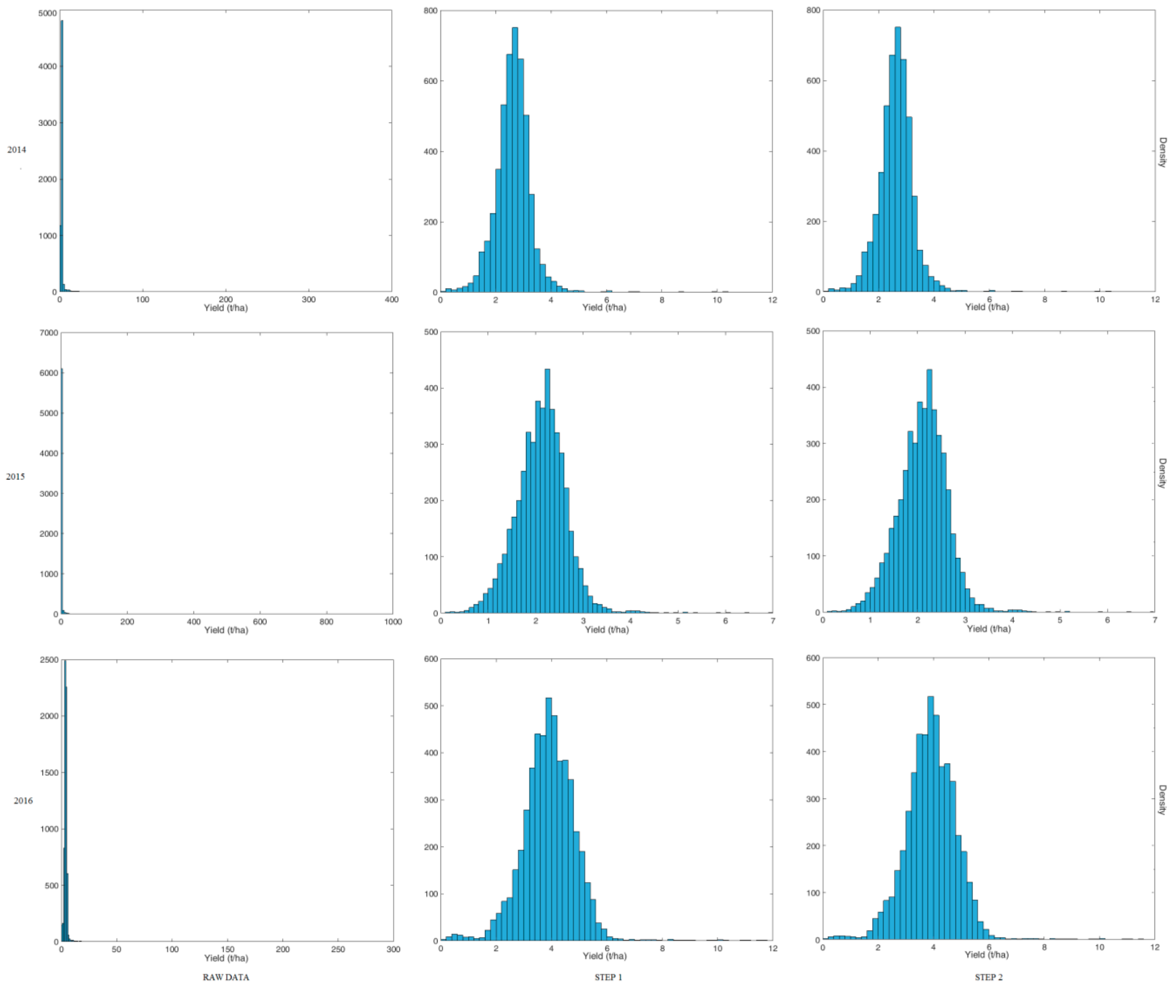

Figure 2. Distribution of yield monitoring datasets for uncleaned and cleaned yield data (data not interpolated).

In fact, after Step1 + Step2 the skewness had values close to zero for 2015 and 2016 crop seasons (Table 2), while for 2014 the final skewness of 2.71 was due to a longer tail on the right side of the data distribution. After Step1 between 24.1% and 26.2% of points were removed, whilst after Step2 a further 1.3% to 2.3% of the dataset was removed. Following the Step1 + Step2 protocol, the percentage of points removed was from 25.9% to 27.1%, close to the range previously reported in the literature [13,47–50].

Figure 3 presents a visual analysis of the location of data removed from each year after both Step1 and Step2: First of all, the highest quantity of removed points came from the filtering of edges, secondly all the data points with overlapping coordinates and lastly, data points identified as outliers through local Moran's index of spatial autocorrelation (Step2).

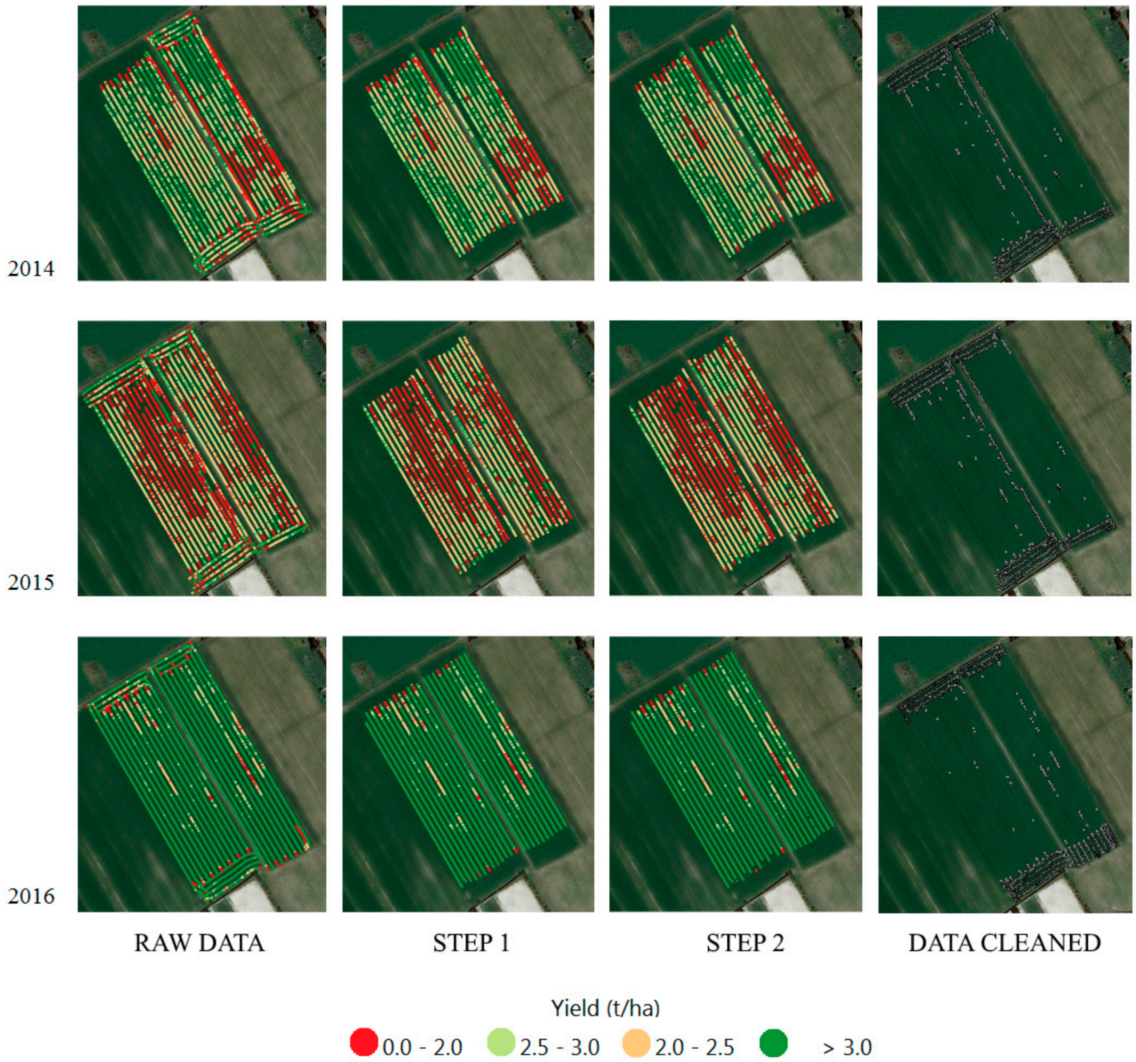

Figure 3. Maps showing yield monitoring datasets: Raw data (left), Step1 and Step2 data (center), data cleaned (right). Raw and Steps 1–2 maps are colored according to quartiles of yield distributions (data not interpolated).

Certainly, the cleaning protocol did not affect the main patterns present in the raw data and allowed both comparison with the sampled yield data and, after interpolation, comparison with the data observed by Landsat-8 (at 30 m of resolution) and Sentinel-2 (at 10 m).

For all three crop seasons, the correlation, its significance and RMSE improved in passing from raw yield monitoring vs. sampled yield to the comparison Step1 + Step2 yield monitoring vs. sampled yield (Table 2). The best improvement was achieved for 2014, where from being non-significant, we found a significant correlation and with a reduction of the RMSE which, however, remained the highest compared to other years. For both 2015 and 2016, the initial correlations between raw data and sampled data were significant and with low RMSE. In any case, the data cleaning procedures improved the performances in terms of both correlation and RMSE.

The different behavior of the 2014 season compared to the other two may be due to intense weeding during the first year of the trial, which caused a large within-field variability of yield.

Given the nature of the comparison between two sets of data that do not refer strictly to the same harvested plants, the worst results obtained for 2014 seem to be clearly linked to the greater variability of within-field yield, unlike crop seasons with uniformly low within-field yield (2015) or uniformly high yield (2016) (Table 3). This corresponds well with Arslan and Colvin [51], who reported that high accuracy cannot be achieved by spot measurements; however, the overall yield trend can be determined. The correlations between spatial data are strongly scale-dependent [52] and of course depend on the coincidence of location between the sampled and monitored data, that in our study is not possible since the hand yield sampling was destructive (before yield mapping).

Table 3. Comparison between yield (t/ha) sampled and monitoring data (mean, max, min and std) (2014–2017).

	2014		**2015**		**2016**		**2017**	
	Sample (t/ha)	**Monitor (t/ha)**	**Sample (t/ha)**	**Monitor (t/ha)**	**Sample (t/ha)**	**Monitor (t/ha)**	**Sample (t/ha)**	**Monitor (t/ha)**
Mean	3.07	2.65	2.31	2.11	3.88	3.90	5.00	N/A
Min	0.42	0.18	0.87	0.15	2.15	0.12	3.23	N/A
Max	5.69	10.48	3.64	6.90	6.01	11.62	7.43	N/A
Std	1.01	1.12	0.57	0.53	0.71	0.91	0.94	N/A

The correlation coefficients found for all three crop seasons (ranging from 0.40 to 0.50) were in general lower but similar to the findings of Ingeli et al. [16]. The latter is the only published paper to have compared two sources of yield data, the hand sampled data as independent variable and yield monitoring data as dependent variable. For five different crop seasons, the authors found correlations ranging between 0.3 to 0.9 but reporting on a small number of hand sampled data (18 + 3 replications) spread over a larger field area (16 ha) unlike our case study with 104 samples in a smaller area (5 ha).

3.2. Yield and NDVI

For the whole period, few Landsat-8 and Sentinel-2 images were used because most of those acquired were useless due to the presence of clouds. For the first two years (2014 and 2015) the images are limited to two in a fairly short time window and in any case always before crop heading stage. In 2016 there are four useful images spread over a much wider period (March–May), while three images are available in 2017 for the same period.

The scientific and operational life of Sentinel-2 started in July 2015, so the useful passages only relate to 2016 and 2017. In 2016 it is possible to use only one image and it was taken at the end of May. In 2017 there are four useful images in a time window similar to that of the Landsat-8 images for 2017 (Table 3).

A comparison of the NDVI with yield monitoring values (Step1 + Step2) (for 2014–2015–2016, Figures 4–7) reveals significant positive linear relationships (r ranging from 0.54 to 0.74) explaining most of the within-field variability in 2014 with the image acquired in April (R^2 = 0.55) and in 2016 with the image acquired in March (R^2 = 0.55). In all other cases, although the correlations are significant, R^2 are lower than 0.5.

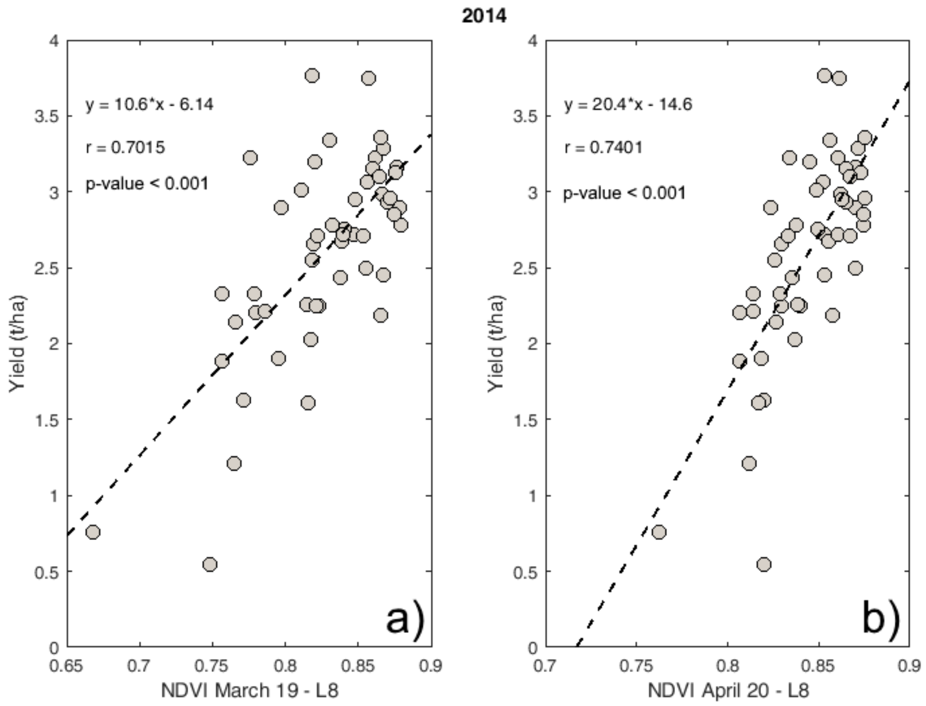

Figure 4. Relationship between observed yield (yield monitor) and NDVI (Landsat-8) for 2013–2014 crop season in (**a**) 19 March and (**b**) 20 April.

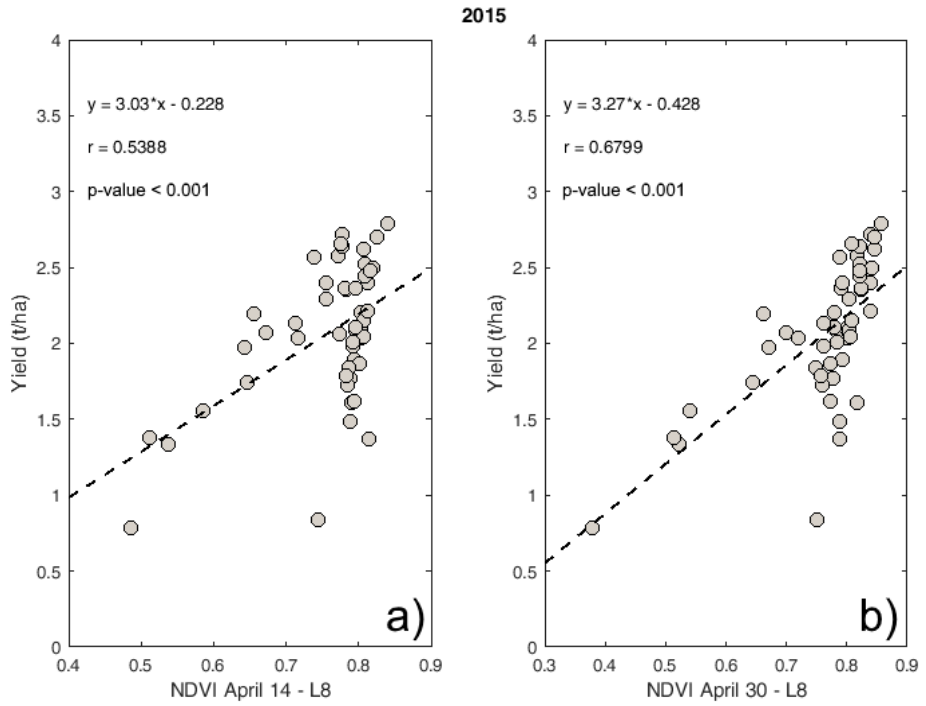

Figure 5. Relationship between observed yield (yield monitor) and NDVI (Landsat-8) for 2014–2015 crop season in (**a**) 14 April and (**b**) 30 April.

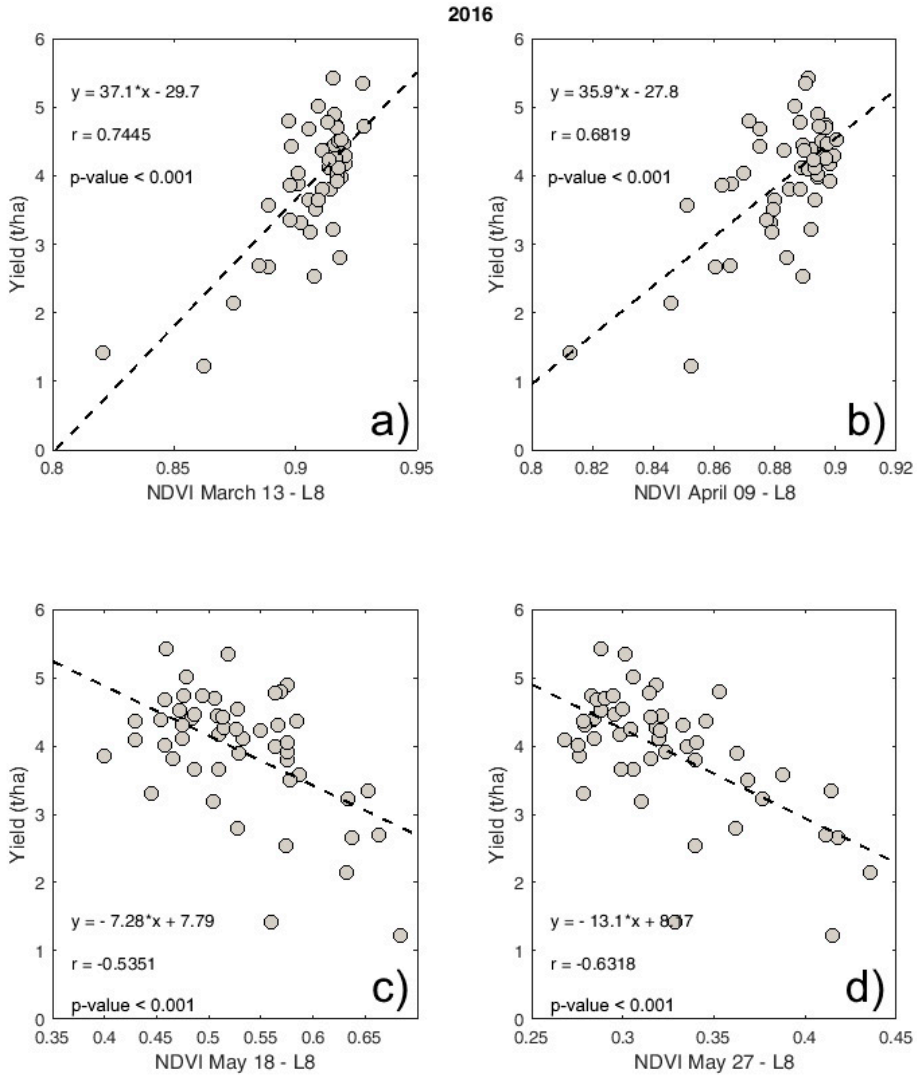

Figure 6. Relationship between observed yield (yield monitor) and NDVI (Landsat-8) for 2015–2016 crop season in (**a**) 13 March, (**b**) 9 April, (**c**) 18 May and (**d**) 27 May.

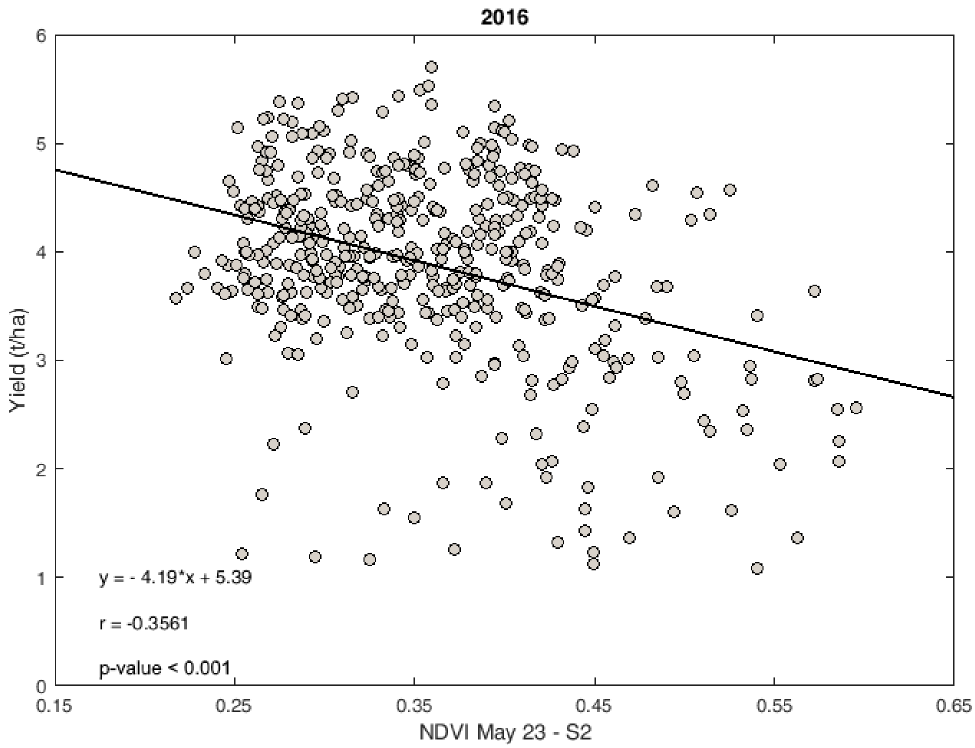

Figure 7. Relationship between observed yield (yield monitor) and NDVI (Sentinel-2) for 2015–2016 crop season.

These results, in terms of both correlations and timing, are in line with Mahey et al. [53]. Freeman et al. [54] found NDVI and wheat grain yield to be highly correlated, establishing the potential to predict yield with remotely sensed data as reported subsequently in several studies for a variety of crop types [55–58].

Freeman et al. [54] also indicated that yield estimates for wheat may be made two months prior to harvest.

Instead, only for 2016, from post-flowering to grain filling, we report weaker but significant negative correlations between NDVI and yield. This is for the Landsat-8 (18 and 27 May, Figure 6) images and the only one available for Sentinel-2 (23 May, Figure 7).

Although negative correlations between NDVI and crop yield are reported in the literature for potato late in the season [55] and for canola, after bolting and once the plants start transitioning to the reproductive stages [59], there are few similar findings for cereal crops when analyzing single or multi cultivars [60–63]. All these latter authors found a negative correlation under severe stress conditions, such as high temperature and drought, during grain filling.

Conversely, in our case study and for 2015–2016 crop season, this unique behavior of NDVI that from strongly positively correlation swings negative to more than −0.6 late in the season is mainly due to opposite climatic conditions (cool-moist) that characterized crop development and above all the period from heading to maturity (Table 4).

Table 4. Climate conditions, phenological length for heading to maturity (H to M) and anthesis to maturity (A to M), leaf area index (LAI) function derivative rate of change for the four crop seasons from anthesis to maturity.

		Number of Days	Total Rainfall (mm)	Air Temperature (°C)	LAI Rate of Change
2014	H to M	79	125.4	20.51	−0.099
	A to M	57	89.6	22.33	
2015	H to M	59	64.0	21.34	−0.142
	A to M	41	64.0	21.64	
2016	H to M	83	129.2	18.88	−0.085
	A to M	64	81.8	19.62	
2017	H to M	67	104.6	19.46	−0.131
	A to M	46	62.4	20.58	

In fact, the longest duration of heading to maturity and anthesis to maturity was observed in 2016 (Table 4) as well as the highest amount of rainfall from heading to maturity (129.2 mm) and lowest mean air temperature both from heading to maturity and anthesis to maturity (18.88 °C and 19.62 °C respectively). These conditions resulted in a general delayed leaf senescence and prolonged late grain filling as a sort of stay green effect [1,64] that is confirmed by the lowest decline rate of LAI in 2016 (Figure 8, Table 4). The derivatives of the modelled LAI function from heading to maturity has a rate of change for 2016 of −0.085, so is lower compared to other years. In the absence of water-stress, as for 2016, stay green is not always correlated with yield (in wheat [65,66] and in sorghum [67]) and can even be associated with reduced yield. For instance, in irrigated wheat and in rice in China, stay green was associated with slow export of leaf carbohydrate to the grain, increased lodging, and harvest difficulties due to delayed ripening, all of which can contribute to reduce yield [68,69]. In our case study, it is likely that this did not occur uniformly due to site-specific soil plant interactions, and the areas within the field that exhibited higher NDVI values during maturation then had translocation problems to the grains. This is confirmed by the fact that the areas with the lowest production (highest NDVI) in 2016 fall in the same low production areas as 2014 and 2015 (Figure 3). Contrary to what happened in 2014, the presence of weeds was not reported for 2016.

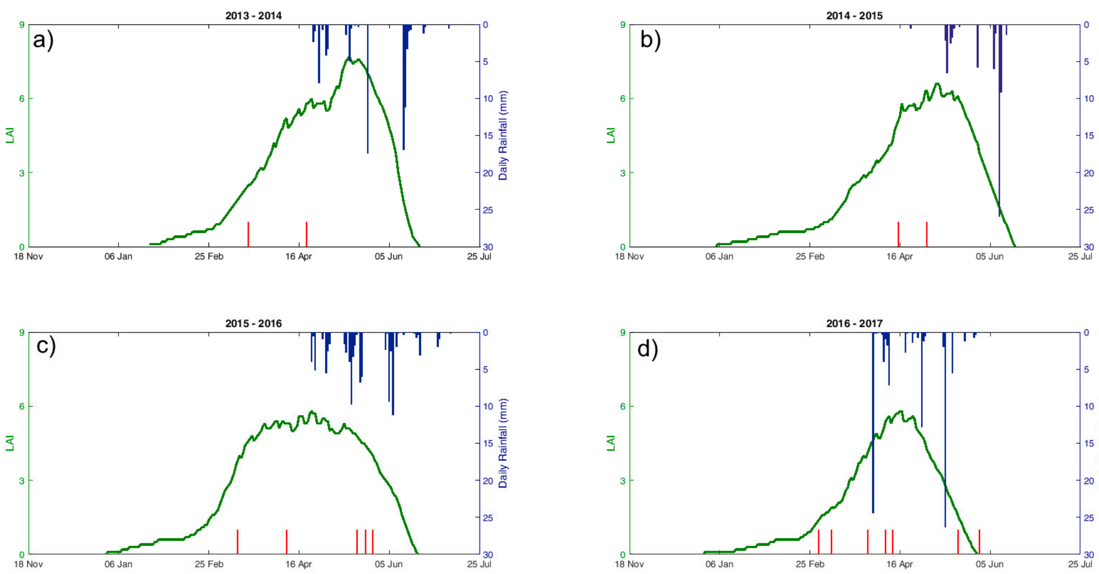

Figure 8. Modelled LAI (green), observed rainfall after heading (blue) and satellite observation (red) for (**a**) 2013–2014, (**b**) 2014–2015, (**c**) 2015–2016 and (**d**) 2016–2017 seasons.

For 2017, having no yield monitoring data, it was possible to compare NDVI data only with hand sampled data (Figures 9 and 10). Also, in this case the highest correlations are observed in the months of March and April, then tend to decrease in May (Sentinel-2, Figure 10) or become non-significant for the Landsat-8 passage in late May (Figure 9). The low and non-significant relationship in late May is probably due to the fact that the drying process had already started unevenly in some areas of the field [33].

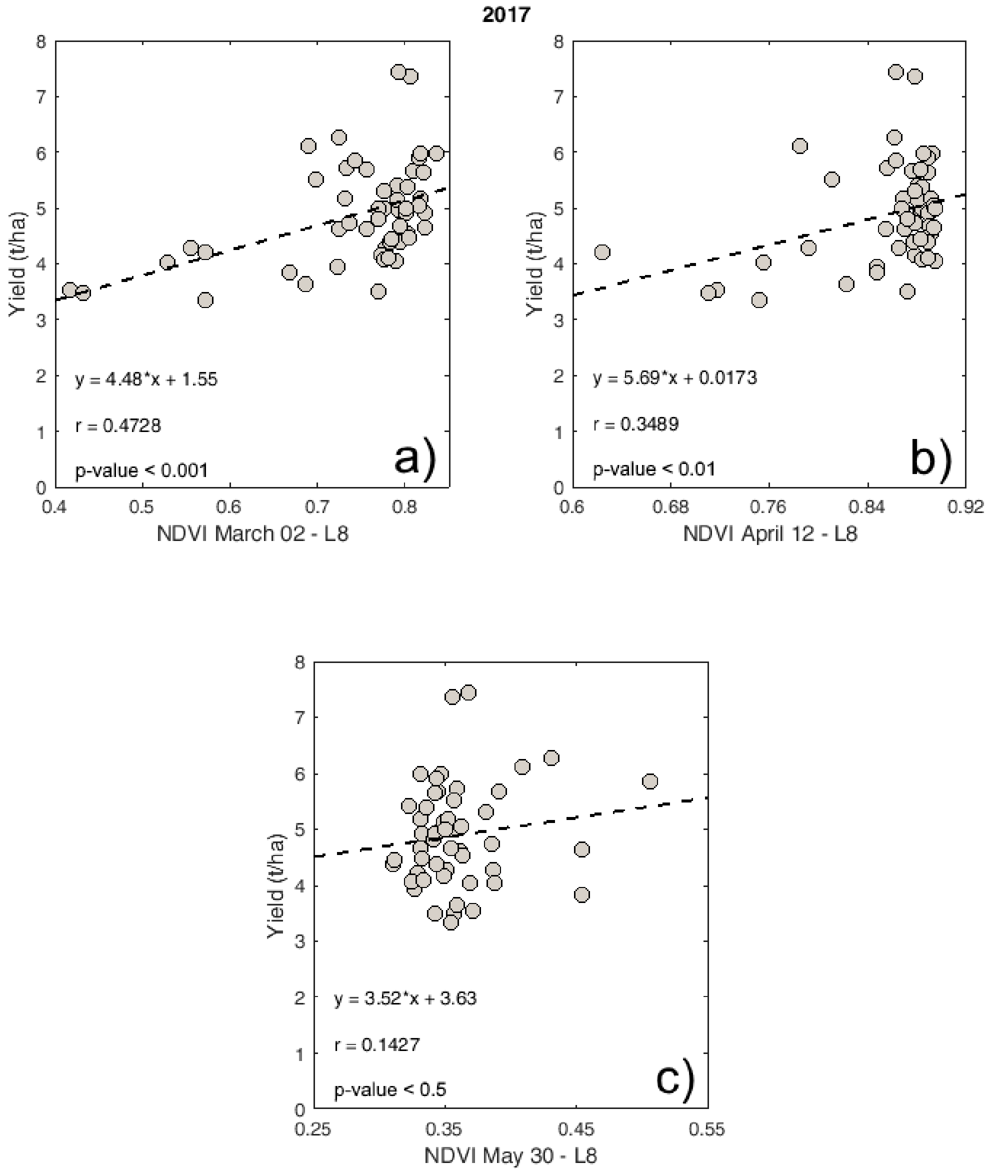

Figure 9. Relationship between observed yield (sampled) and NDVI (Landsat-8) for 2016–2017 crop season in (**a**) 2 March, (**b**) 12 April and (**c**) 30 May.

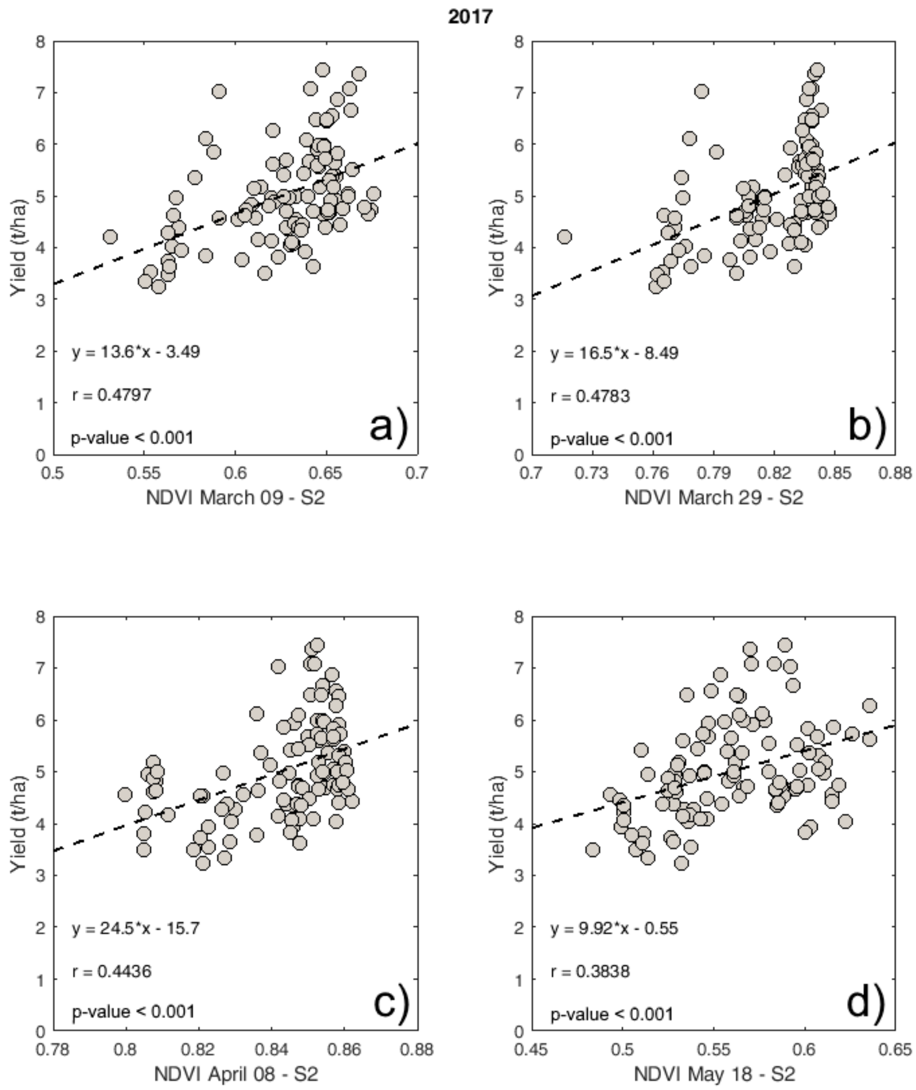

Figure 10. Relationship between observed yield (sampled) and NDVI (Sentinel-2) for 2016–2017 crop season in (**a**) 9 March, (**b**) 29 March, (**c**) 8 April and (**d**) 18 May.

Unfortunately, all the empirical relationships determined over the whole study period cannot be applied elsewhere, since a universal conversion from vegetation indices to yield values does not exist, as pointed out by Georgi et al. [9]. Many efforts have been made to determine this relationship [17,70,71], with results indicating that replicability is mostly limited by crop type and climate zone, confirming our case study findings. Our results highlight the potential use of remote sensing imagery (Sentinel-2 and Landsat-8) for within-field and interannual durum wheat yield assessment under Mediterranean conditions. Although it is not possible to retrieve absolute yield values, the results show the capacity of the NDVI to describe within-field yield levels providing objective criteria, also in terms of potential performance, on which to base nutrient management zones for soil sampling and variable-rate nutrient application, especially thanks to the availability of multiple years of data. This is also facilitated by the fact that, even if multiple surveys are done during crop development, NDVI and yield are strongly correlated at stem elongation and heading stages, which are among the most important for agronomic management to support and improve durum wheat yield and quality.

4. Conclusions

The first part of the study is mainly practice oriented, testing a state of the art protocol for error removal from yield monitoring data and comparing the cleaning map with hand field sampling data. The cleaning process improved measurement accuracy of spatial variability, which is key for adopting precision farming techniques to make daily fieldwork more efficient and increase agricultural productivity. In light of this, in the second part of the study, the usefulness of remote sensing information collected during the optimal period for characterizing within-field spatial variability of durum wheat productivity has been assessed.

Findings suggest that the best time to relate NDVI to durum wheat yields under rainfed conditions in the Mediterranean area is the period leading up to 90–60 days before harvest (March–April). At the same time the results, based on a four year yield dataset, support the conclusion that a unique NDVI-yield relationship cannot be achieved and applied to different years or environments, but year by year can suggest the best management approach while taking farmers' requirements into account.

Additional research is needed in the future to: (i) test different methods of comparing heterogeneous data (different supports, spatial resolution), (ii) address the performance of other VIs and promote them among end users. Furthermore, in case of long periods between satellite images due to cloud cover, the use of a crop simulation model has proved to be of fundamental importance to simulate the crop stage and growth conditions and better understand differences underlying correlations between yield and VIs.

Author Contributions: A.V.V. and A.C. designed the experiment. P.T., A.C., S.F.D.G., A.V.V., D.V. and A.M. formulated the research methodology and wrote the manuscript. P.T., S.F.D.G. and A.M. provided necessary data analysis. All authors reviewed and edited the draft.

Funding: This research was funded by Italian P.O.N. "Ricerca e competitività" 2007–2013 for convergence Regions (grant number: CTN01_00230_450760, D.D. 257/Ric/2012 of "Ministero dell'Istruzione, dell'Università e della Ricerca"): "Sostenibilità della Filiera Agroalimentare Italiana" (SO.FI.A.).

Conflicts of Interest: The authors declare no conflict of interest.

References

1. Toscano, P.; Gioli, B.; Genesio, L.; Vaccari, F.P.; Miglietta, F.; Zaldei, A.; Crisci, A.; Ferrari, E.; Bertuzzi, F.; La Cava, P.; et al. Durum wheat quality prediction in Mediterranean environments: From local to regional scale. *Eur. J. Agron.* **2014**, *61*, 1–9. [CrossRef]
2. Royo, C.; Nazco, R.; Villegas, D. The climate of the zone of origin of Mediterranean durum wheat (Triticum durum Desf.) landraces affects their agronomic performance. *Genet. Resour. Crop Evol.* **2014**, *61*, 1345–1358. [CrossRef]
3. Tedone, L.; Alhajj Ali, S.; Verdini, L.; De Mastro, G. Nitrogen management strategy for optimizing agronomic and environmental performance of rainfed durum wheat under Mediterranean climate. *J. Clean. Prod.* **2018**, *172*, 2058–2074. [CrossRef]
4. Soddu, A.; Deidda, R.; Marrocu, M.; Meloni, R.; Paniconi, C.; Ludwig, R.; Sodde, M.; Mascaro, G.; Perra, E. Climate Variability and Durum Wheat Adaptation Using the AquaCrop Model in Southern Sardinia. *Procedia Environ. Sci.* **2013**, *19*, 830–835. [CrossRef]
5. Toscano, P.; Ranieri, R.; Matese, A.; Vaccari, F.P.; Gioli, B.; Zaldei, A.; Silvestri, M.; Ronchi, C.; La Cava, P.; Porter, J.R.; et al. Durum wheat modeling: The Delphi system, 11 years of observations in Italy. *Eur. J. Agron.* **2012**, *43*, 108–118. [CrossRef]
6. Giuliani, M.M.; Giuzio, L.; de Caro, A.; Flagella, Z. Relationships between nitrogen utilization and grain technological quality in durum wheat: II. Grain yield and quality. *Agron. J.* **2011**, *103*, 1668–1675. [CrossRef]
7. Bowman, M.S.; Zilberman, D. Economic factors affecting diversified farming systems. *Ecol. Soc.* **2013**, *18*, 33. [CrossRef]
8. Mulla, D.J. Twenty five years of remote sensing in precision agriculture: Key advances and remaining knowledge gaps. *Biosyst. Eng.* **2013**, *114*, 358–371. [CrossRef]
9. Georgi, C.; Spengler, D.; Itzerott, S.; Kleinschmit, B. Automatic delineation algorithm for site-specific management zones based on satellite remote sensing data. *Precis. Agric.* **2018**, *19*, 684–707. [CrossRef]
10. Thilakarathna, M.; Raizada, M. Challenges in Using Precision Agriculture to Optimize Symbiotic Nitrogen Fixation in Legumes: Progress, Limitations, and Future Improvements Needed in Diagnostic Testing. *Agronomy* **2018**, *8*, 78. [CrossRef]

11. Ping, J.L.; Dobermann, A. Processing of yield map data. *Precis. Agric.* **2005**, *6*, 193–212. [CrossRef]
12. Thöle, H.; Richter, C.; Ehlert, D. Strategy of statistical model selection for precision farming on-farm experiments. *Precis. Agric.* **2013**, *14*, 434–449. [CrossRef]
13. Vega, A.; Córdoba, M.; Castro-Franco, M.; Balzarini, M. Protocol for automating error removal from yield maps. *Precis. Agric.* 2019. [CrossRef]
14. Lyle, G.; Bryan, B.A.; Ostendorf, B. Post-processing methods to eliminate erroneous grain yield measurements: Review and directions for future development. *Precis. Agric.* **2014**, *15*, 377–402. [CrossRef]
15. Arslan, S. A grain flow model to simulate grain yield sensor response. *Sensors* **2008**, *8*, 952–962. [CrossRef]
16. Ingeli, M.; Galambošová, J.; Macák, M.; Rataj, V. Study on Correlation of Data from Yield Monitoring System and Hand Samples. *Acta Technol. Agric.* **2015**, *18*, 10–13. [CrossRef]
17. Doraiswamy, P.C.; Hatfield, J.L.; Jackson, T.J.; Akhmedov, B.; Prueger, J.; Stern, A. Crop condition and yield simulations using Landsat and MODIS. *Remote Sens. Environ.* **2004**, *92*, 548–559. [CrossRef]
18. Funk, C.; Budde, M.E. Phenologically-tuned MODIS NDVI-based production anomaly estimates for Zimbabwe. *Remote Sens. Environ.* **2009**, *113*, 115–125. [CrossRef]
19. Johnson, D.M. An assessment of pre- and within-season remotely sensed variables for forecasting corn and soybean yields in the United States. *Remote Sens. Environ.* **2014**, *141*, 116–128. [CrossRef]
20. Gao, F.; Anderson, M.; Daughtry, C.; Johnson, D. Assessing the variability of corn and soybean yields in central Iowa using high spatiotemporal resolution multi-satellite imagery. *Remote Sens.* **2018**, *10*, 1489. [CrossRef]
21. Skakun, S.; Vermote, E.; Roger, J.-C.; Franch, B. Combined Use of Landsat-8 and Sentinel-2A Images for Winter Crop Mapping and Winter Wheat Yield Assessment at Regional Scale. *AIMS Geosci.* **2017**, *3*, 163–186. [CrossRef] [PubMed]
22. Azzari, G.; Jain, M.; Lobell, D.B. Towards fine resolution global maps of crop yields: Testing multiple methods and satellites in three countries. *Remote Sens. Environ.* **2017**, *202*, 129–141. [CrossRef]
23. Jin, Z.; Azzari, G.; Lobell, D.B. Improving the accuracy of satellite-based high-resolution yield estimation: A test of multiple scalable approaches. *Agric. For. Meteorol.* **2017**, *247*, 207–220. [CrossRef]
24. Zhong, L.; Yu, L.; Li, X.; Hu, L.; Gong, P. Rapid corn and soybean mapping in US Corn Belt and neighboring areas. *Sci. Rep.* **2016**, *6*, 36240. [CrossRef] [PubMed]
25. Lambert, M.J.; Traoré, P.C.S.; Blaes, X.; Baret, P.; Defourny, P. Estimating smallholder crops production at village level from Sentinel-2 time series in Mali's cotton belt. *Remote Sens. Environ.* **2018**, *216*, 647–657. [CrossRef]
26. Newton, I.H.; Tariqul Islam, A.F.M.; Saiful Islam, A.K.M.; Tarekul Islam, G.M.; Tahsin, A.; Razzaque, S. Yield Prediction Model for Potato Using Landsat Time Series Images Driven Vegetation Indices. *Remote Sens. Earth Syst. Sci.* **2018**, *1*, 29–38. [CrossRef]
27. López-Lozano, R.; Casterad, M.A.; Herrero, J. Site-specific management units in a commercial maize plot delineated using very high resolution remote sensing and soil properties mapping. *Comput. Electron. Agric.* **2010**, *73*, 219–229. [CrossRef]
28. Nawar, S.; Corstanje, R.; Halcro, G.; Mulla, D.; Mouazen, A.M. Delineation of Soil Management Zones for Variable-Rate Fertilization: A Review. In *Advances in Agronomy*; Academic Press: Cambridge, MA, USA, 2017; pp. 175–245.
29. Han, J.; Wei, C.; Chen, Y.; Liu, W.; Song, P.; Zhang, D.; Wang, A.; Song, X.; Wang, X.; Huang, J. Mapping above-ground biomass ofwinter oilseed rape using high spatial resolution satellite data at parcel scale under waterlogging conditions. *Remote Sens.* **2017**, *9*, 3. [CrossRef]
30. Dong, T.; Shang, J.; Liu, J.; Qian, B.; Jing, Q.; Ma, B.; Huffman, T.; Geng, X.; Sow, A.; Shi, Y.; et al. Using RapidEye imagery to identify within-field variability of crop growth and yield in Ontario, Canada. *Precis. Agric.* **2019**, 1–20. [CrossRef]
31. Maes, W.H.; Steppe, K. Perspectives for Remote Sensing with Unmanned Aerial Vehicles in Precision Agriculture. *Trends Plant Sci.* **2019**, *24*, 152–164. [CrossRef]
32. Al-Gaadi, K.A.; Hassaballa, A.A.; Tola, E.; Kayad, A.G.; Madugundu, R.; Alblewi, B.; Assiri, F. Prediction of potato crop yield using precision agriculture techniques. *PLoS ONE* **2016**, *11*, e0162219. [CrossRef] [PubMed]
33. Escolà, A.; Badia, N.; Arnó, J.; Martínez-Casasnovas, J.A. Using Sentinel-2 images to implement Precision Agriculture techniques in large arable fields: First results of a case study. *Adv. Anim. Biosci.* **2017**, *8*, 377–382. [CrossRef]

34. Jeppesen, J.H.; Jacobsen, R.H.; Jørgensen, R.N.; Halberg, A.; Toftegaard, T.S. Identification of High-Variation Fields based on Open Satellite Imagery. *Adv. Anim. Biosci.* **2017**, *8*, 388–393. [CrossRef]
35. Soil Survey Staff. *Soil Taxonomy: A Basic System of Soil Classification for Making and Interpreting Soil Surveys*, 2nd ed.; USDA-Soil Survey Staff, Ed.; United States Department of Agriculture: Washington, DC, USA, 1999.
36. Ventrella, D.; Stellacci, A.M.; Castrignanò, A.; Charfeddine, M.; Castellini, M. Effects of crop residue management on winter durum wheat productivity in a long term experiment in Southern Italy. *Eur. J. Agron.* **2016**, *77*, 188–198. [CrossRef]
37. Deering, D.W. Rangeland reflectance characteristics measured by aircraft and spacecraft sensors. *Diss. Abstr. Int. B* **1979**, *39*, 3081–3082.
38. Anselin, L.; Syabri, I.; Kho, Y. GeoDa: An introduction to spatial data analysis. *Geogr. Anal.* **2006**, *38*, 5–22. [CrossRef]
39. QGIS. QGIS Geographic Information System. Open Source Geospatial Foundation Project. 2017. Available online: https://qgis.org/en/site/(accessed on 8 August 2019).
40. Minasny, B.; McBratney, A.B.; Whelan, B.M. *VESPER Version 1.62*, Australian Centre for Precision Agriculture, The University of Sydney: Sydney, Australia, 2005.
41. Mathworks Inc. *MATLAB and Statistics Toolbox Release*, Mathworks Inc.: Natick, MA, USA, 2016.
42. Amelin, L. Local Indicators of Spatial Association-LISA. *Geogr. Anal.* **1995**, *27*, 93–115.
43. Anselin, L. The Moran Scatterplot as an ESDA Tool to Assess Local Instability in Spatial Association. In *Spatial Analytical Perspectives on GIS*; Fischer, M., Scholten, H., Unwin, D., Eds.; Taylor and Francis: London, UK, 1996; pp. 111–125.
44. Porter, J.R.; Porter, J.R. AFRCWHEAT2 A model of the growth and development of wheat incorporating responses to water and nitrogen. *Eur. J. Agron.* **1993**, *2*, 69–82. [CrossRef]
45. Su, L.; Wang, Q.; Wang, C.; Shan, Y. Simulation models of leaf area index and yield for cotton grown with different soil conditioners. *PLoS ONE* **2015**, *10*, e0141835. [CrossRef] [PubMed]
46. Wang, M.H. Field Information Collection and Process Technology. *Agric. Mech.* **1999**, *7*, 22–24.
47. Leroux, C.; Jones, H.; Clenet, A.; Dreux, B.; Becu, M.; Tisseyre, B. A general method to filter out defective spatial observations from yield mapping datasets. *Precis. Agric.* **2018**, *19*, 789–808. [CrossRef]
48. Sudduth, K.A.; Drummond, S.T. Yield editor: Software for removing errors from crop yield maps. *Agron. J.* **2007**, *99*, 1471–1482. [CrossRef]
49. Simbahan, G.C.; Dobermann, A.; Ping, J.L. Site-specific management—Screening yield monitor data improves grain yield maps. *Agron. J.* **2004**, *96*, 1091–1102. [CrossRef]
50. Sun, W.; Whelan, B.; McBratney, A.B.; Minasny, B. An integrated framework for software to provide yield data cleaning and estimation of an opportunity index for site-specific crop management. *Precis. Agric.* **2013**, *14*, 376–391. [CrossRef]
51. Arslan, S.; Colvin, T.S. Grain yield mapping: Yield sensing, yield reconstruction, and errors. *Precis. Agric.* **2002**, *3*, 135–154. [CrossRef]
52. Young, L.J.; Gotway, C.A. Linking spatial data from different sources: The effects of change of support. *Stoch. Environ. Res. Risk Assess.* **2007**, *21*, 589–600. [CrossRef]
53. Mahey, R.K.; Singh, R.; Sidhu, S.S.; Narang, R.S. The use of remote sensing to assess the effects of water stress on wheat. *Exp. Agric.* **1991**, *27*, 423–429. [CrossRef]
54. Freeman, K.W.; Raun, W.R.; Johnson, G.V.; Mullen, R.W.; Stone, M.L.; Solie, J.B. Late-season prediction of wheat grain yield and grain protein. *Commun. Soil Sci. Plant Anal.* **2003**, *34*, 1837–1852. [CrossRef]
55. Johnson, D.M. A comprehensive assessment of the correlations between field crop yields and commonly used MODIS products. *Int. J. Appl. Earth Obs. Geoinf.* **2016**, *52*, 65–81. [CrossRef]
56. Kogan, F.; Kussul, N.; Adamenko, T.; Skakun, S.; Kravchenko, O.; Kryvobok, O.; Shelestov, A.; Kolotii, A.; Kussul, O.; Lavrenyuk, A. Winter wheat yield forecasting in Ukraine based on Earth observation, meteorologicaldata and biophysical models. *Int. J. Appl. Earth Obs. Geoinf.* **2013**, *23*, 192–203. [CrossRef]
57. Mkhabela, M.S.; Bullock, P.; Raj, S.; Wang, S.; Yang, Y. Crop yield forecasting on the Canadian Prairies using MODIS NDVI data. *Agric. For. Meteorol.* **2011**, *151*, 385–393. [CrossRef]
58. Becker-Reshef, I.; Vermote, E.; Lindeman, M.; Justice, C. A generalized regression-based model for forecasting winter wheat yields in Kansas and Ukraine using MODIS data. *Remote Sens. Environ.* **2010**, *114*, 1312–1323. [CrossRef]

59. Weber, J.; Gazali, I. 2017 Annual Report for the Agriculture Demonstration of Practices and Technologies (ADOPT). 2017. Available online: https://sa241e23dba898335.jimcontent.com/download/version/1526570262/module/10558155383/name/20150375%20ADOPT%20Report%20Nitrogen%20Benefits%20of%20adapted%20grain%20legumes%20to%20succeeding%20crops%20in%20NW%20SK.pdf (accessed on 8 August 2019).
60. Kyratzis, A.C.; Skarlatos, D.P.; Menexes, G.C. Assessment of Vegetation Indices Derived by UAV Imagery for Durum Wheat Phenotyping under a Water Limited and Heat Stressed Mediterranean Environment. *Front. Plant Sci.* **2017**, *8*, 1–14. [CrossRef] [PubMed]
61. Lopes, M.S.; Saglam, D.; Ozdogan, M.; Reynolds, M. Traits associated with winter wheat grain yield in Central and West Asia. *J. Integr. Plant Biol.* **2014**, *56*, 673–683. [CrossRef]
62. Corresponding, J.B.; Casadesus, J.; Nachit, M.M.; Araus, J.L. Factors affecting the grain yield predicting attributes of spectral reflectance indices in durum wheat: growing conditions, genotype variability and date of measurement. *Int. J. Remote Sens.* **2005**, *26*, 2337–2358.
63. Rutkoski, J.; Poland, J.; Mondal, S.; Autrique, E.; Pérez, L.G.; Crossa, J.; Reynolds, M.; Singh, R. Canopy Temperature and Vegetation Indices from High-Throughput Phenotyping Improve Accuracy of Pedigree and Genomic Selection for Grain Yield in Wheat. *Genes Genomes Genet.* **2016**, *6*, 2799–2808. [CrossRef]
64. Spano, G.; Di Fonzo, N.; Perrotta, C.; Platani, C.; Ronga, G.; Lawlor, D.W.; Napier, J.A. Physiological characterization of 'stay green' mutants in durum wheat. *J. Exp. Bot.* **2003**, *54*, 1415–1420. [CrossRef]
65. Lopes, M.S.; Reynolds, M.P. Stay-green in spring wheat can be determined by spectral reflectance measurements (normalized difference vegetation index) independently from phenology. *J. Exp. Bot.* **2012**, *63*, 3789–3798. [CrossRef]
66. Gregersen, P.L.; Culetic, A.; Boschian, L.; Krupinska, K. Plant senescence and crop productivity. *Plant Mol. Biol.* **2013**, *82*, 603–622. [CrossRef] [PubMed]
67. Jordan, D.R.; Hunt, C.H.; Cruickshank, A.W.; Borrell, A.K.; Henzell, R.G. The relationship between the stay-green trait and grain yield in elite sorghum hybrids grown in a range of environments. *Crop Sci.* **2012**, *52*, 1153–1161. [CrossRef]
68. Gong, Y.-H.; Zhang, J.; Gao, J.-F.; Lu, J.-Y.; Wang, J.-R. Slow Export of Photoassimilate from Stay-Green Leaves during Late Grain-Filling Stage in Hybrid Winter Wheat (Triticum aestivum L.). *J. Agron. Crop Sci.* **2005**, *191*, 292–299. [CrossRef]
69. Yang, J.; Zhang, J. Grain filling of cereals under soil drying. *New Phytol.* **2006**, *169*, 223–236. [CrossRef] [PubMed]
70. Shanahan, J.F.; Schepers, J.S.; Francis, D.D.; Varvel, G.E.; Wilhelm, W.W.; Tringe, J.M.; Schlemmer, M.R.; Major, D.J. Use of remote-sensing imagery to estimate corn grain yield. *Agron. J.* **2001**, *93*, 583–589. [CrossRef]
71. Dalla Marta, A.; Grifoni, D.; Mancini, M.; Orlando, F.; Guasconi, F.; Orlandini, S. Durum wheat in-field monitoring and early-yield prediction: Assessment of potential use of high resolution satellite imagery in a hilly area of Tuscany, Central Italy. *J. Agric. Sci.* **2015**, *153*, 68–77. [CrossRef]